ChemComm

COMMUNICATION

View Article Online
View Journal | View Issue

Check for updates

Cite this: *Chem. Commun.*, 2026, **62**, 8027

Received 13th February 2026,
Accepted 25th March 2026

DOI: 10.1039/d6cc00576d

rsc.li/chemcomm

Open Access Article. Published on 30 March 2026. Downloaded on 5/31/2026 11:00:37 AM.
This article is licensed under a Creative Commons Attribution 3.0 Unported Licence.

Merging platinahelicene and nanographene: a strategy for circularly polarized phosphorescence in the near-infrared (NIR)

Wenying Cui, [ab] Huimin Zhou,[b] Thierry Roisnel,[a] Nicolas Vanthuyne, [c] Chengshuo Shen,[b] Joachim Grzybowski, [d] J. A. Gareth Williams, [e] Monika Srebro-Hooper, *[d] Yohan Gisbert *[a] and Jeanne Crassous *[a]

We present the first integration of a platinahelicene within a nanographene (NG), giving access to near-infrared circularly polarized phosphorescence with dissymmetry factors g_{lum} reaching 4 × 10^{-3}. For comparison, a novel NG featuring a borahelicene displayed a blue-green circularly polarized fluorescence with g_{lum} = 6 × 10^{-4}.

Over the past two decades, the development of nanographene (NG)-type molecules has experienced tremendous growth thanks to the introduction of highly efficient synthetic methodologies leading to diverse molecular architectures, including the incorporation of heteroatoms and chirality within the NG scaffold.[1–6] This rapidly evolving research field now provides access to sophisticated chiral molecular materials with specific chiroptical activities in both ground and excited states (electronic circular dichroism, ECD; and circularly polarized luminescence, CPL respectively).[7–12] However, achieving CPL in the near-infrared (NIR) remains a significant challenge with such materials: very few chiral NG-type molecules emit CPL above 750 nm.[13–16] Such bathochromically shifted emission typically requires an extended π-conjugated system, involving sophisticated molecular architectures embedding multiple NG units, whose synthesis remains highly specific and challenging (Fig. 1a). We envisaged that the introduction of a metal[17,18] (*e.g.*, Fig. 1b) could offer a straightforward alternative approach to achieving NIR CPL emission in NGs. Platinum has a high spin–orbit coupling (SOC) constant that, in cyclometalated complexes in particular, can promote intersystem crossing and subsequent phosphorescence from triplet excited states.[19,20] The association of a helically chiral nanographene with a platinum center may thus enable the chiroptical properties associated with the organic structure to be combined with room-temperature phosphorescence in the visible or NIR spectral regions.[21] In line with this concept, platinum(II) helicene complexes – or "platinahelicenes" – have been developed that display circularly polarized, red phosphorescence at room temperature.[22–27] In this communication, we describe the first preparation of helically chiral NGs that incorporate a heavy metal, namely platinum (**NG1**, Fig. 1c, left), and show how the

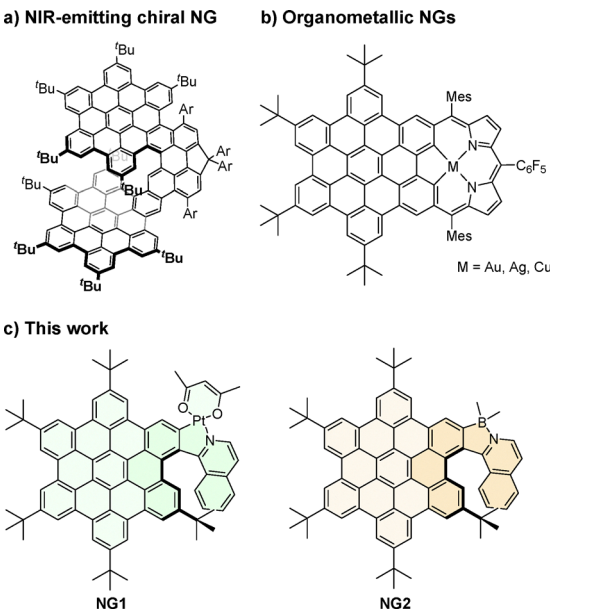

Fig. 1 (a) A fully organic, NIR-emitting, chiral NG featuring extended π conjugation,[13] (b) achiral organometallic nanographenes,[17] and (c) the first helically chiral organometallic nanographene (left) and its analogue featuring a boron atom instead of the platinum center (right) presented in this work.

[a] *Univ Rennes, CNRS, ISCR (Institut des Sciences Chimiques de Rennes) – UMR 6226, F-35000, Rennes, France. E-mail: yohan.gisbert@univ-rennes.fr, jeanne.crassous@univ-rennes.fr*
[b] *School of Chemistry and Chemical Engineering, Zhejiang Sci-Tech University, Hangzhou 310018, China*
[c] *Aix Marseille Univ, CNRS, Centrale Med, FSCM, Marseille 13013, France*
[d] *Faculty of Chemistry, Jagiellonian University, Gronostajowa 2, 30-387, Krakow, Poland. E-mail: srebro@chemia.uj.edu.pl*
[e] *Department of Chemistry, University of Durham, Durham, DH1 3LE, UK*

Open Access Article. Published on 30 March 2026. Downloaded on 5/31/2026 11:00:37 AM.
This article is licensed under a Creative Commons Attribution 3.0 Unported Licence.

straightforward combination of NG and platinahelicene within the same scaffold enables direct access to novel, helically chiral architectures that display CPL activity in the NIR. For comparison, the incorporation of boron[28–32] in place of Pt(II) was carried out with the same NG scaffold (**NG2**, Fig. 1c, right), yielding a blue-green, fluorescent CPL emitter.

The platinum-containing helical nanographene **NG1** was prepared following a 7-step synthetic sequence with 16% overall yield (Scheme 1). Sonogashira cross-coupling of 4-*tert*-butylphenylacetylene[33] and 3-bromoiodobenzene gave diarylacetylene **1**, and subsequent Diels–Alder cycloaddition with 2,3,4,5-tetrakis(4-*tert*-butylphenyl)cyclopentadienone[34] **2**, followed by an *in-situ* chelotropic decarbonylation, yielded the hexaarylbenzene **3**. The latter was subjected to a Scholl cyclodehydrogenation with $FeCl_3/CH_3NO_2$, affording the brominated hexabenzocoronene derivative **4** in 84% yield, corresponding to the concomitant formation of five C–C bonds. Subsequent Miyaura borylation yielded the corresponding pinacol boronic ester **5**, which was then subjected to a Suzuki–Miyaura cross-coupling with 1-bromoisoquinoline **6** to afford the key N^CH proligand **7**, featuring both hexabenzocoronene (NG) and isoquinoline fragments. The platinum-containing helical nanographene **NG1** was prepared from **7** by cycloplatination with $Pt(dmso)_2Cl_2$ followed by a ligand exchange with sodium acetylacetonate to afford **NG1** as a deep-red solid. It was formed as a racemic mixture, from which the (*P*) and (*M*) enantiomers were isolated with an ee > 99% by preparative chiral HPLC (see Section S7 of the SI for details).

The proligand **7** was also used to prepare the metal-free analogue **NG2**, featuring a boron atom instead of the platinum center, by reaction with boron tribromide under basic conditions, followed by methylation at the boron center with trimethylaluminium to afford **NG2** as a bright orange solid in 60% overall yield. Subsequent HPLC separation afforded both enantiomers of **NG2** with ee > 99%.

The structures of **NG1** and **NG2** were unambiguously confirmed by high-resolution mass spectrometry (HRMS) and $^1H/^{13}C$ NMR spectroscopy. Furthermore, the ^{195}Pt NMR of **NG1** displayed a single signal at −2790 ppm, which falls within the expected range for such (N^C)Pt(II) complexes. Single crystals of **NG1** suitable for X-ray diffraction were obtained by slow evaporation of a CH_2Cl_2/pentane solution of **NG1**, which crystallized in the *C*2/c space group (Scheme 1 and SI Section S5). The helicity of **NG1** (angle between the planes of the terminal helicenic rings) is 39.35°, significantly lower than those of carbo[6]helicene (58.5°)[35] and the one observed for a simpler (N^C)platina-[6]helicene (52.3°).[23] This reduction is likely due to stabilizing, attractive, van der Waals/CH-π interactions between the quinoline moiety and the neighboring bulky *tert*-butyl group (Fig. S17 and S29). The **NG1** molecules pack in separated pairs in the studied crystal, with a short Pt···Pt distance of 3.297 Å indicative of metallophilic interactions (Fig. S31). In line with findings for related systems,[20,36] the nucleus-independent chemical shift (NICS) and anisotropy of the induced current density (AICD) analyses (Scheme 1 and

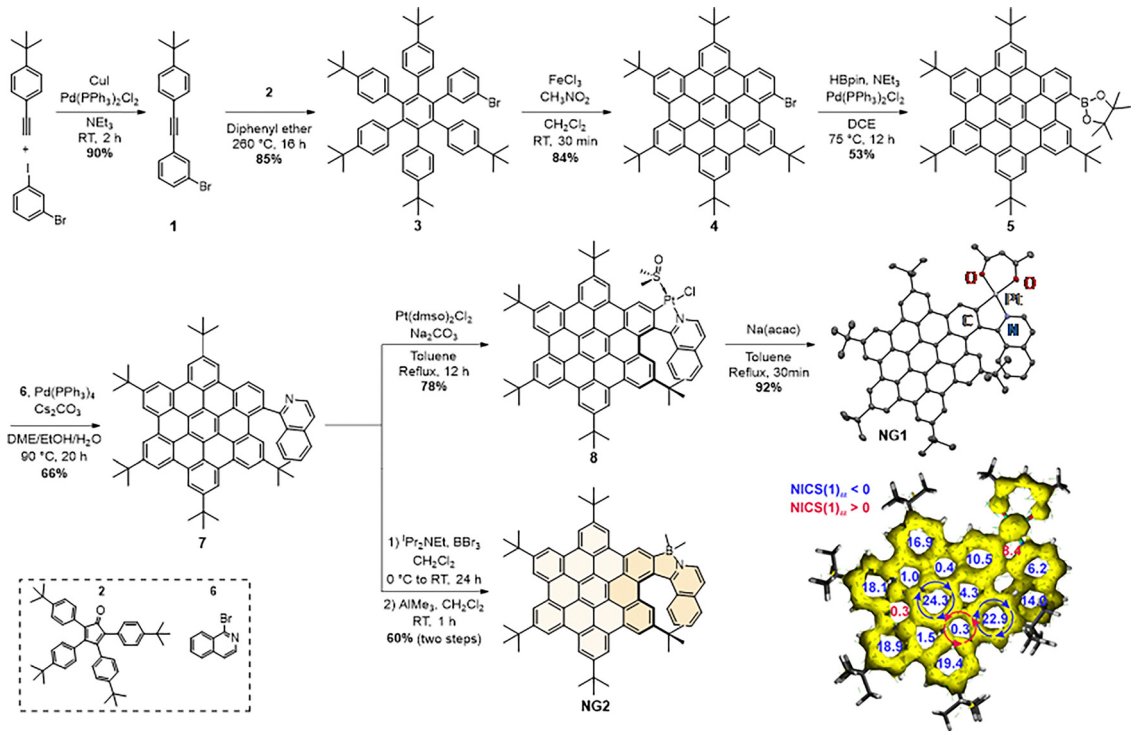

Scheme 1 Synthesis of helically chiral nanographenes **NG1** and **NG2**. ORTEP view of the molecular structure of **NG1**, obtained from a racemic crystal (only the (*P*) enantiomer is shown). Thermal ellipsoids are drawn at 50% probability level. Hydrogen atoms and disorder are omitted for clarity. Calculated AICD plot for **NG1** (0.05 au, arrows indicating the directions of the induced ring current, blue/red = clockwise (diatropic)/counterclockwise (paratropic)) along with the color-coded average $NICS(1)_{zz}$ absolute values (ppm, blue/red = negative/positive).

 This journal is © The Royal Society of Chemistry 2026

Open Access Article. Published on 30 March 2026. Downloaded on 5/31/2026 11:00:37 AM.
This article is licensed under a Creative Commons Attribution 3.0 Unported Licence.

SI Section S4), demonstrated extended π-delocalization and aromatic stabilization across the peripheral rings of the NG core. It also showed localized aromaticity at the center of the NG and on the quinoline moiety (evidenced by diatropic π-electron ring currents and large negative NICS values), as well as non-aromatic character of the platina- and boracycles (positive NICSs); however, a visible involvement of Pt(II) electrons in the induced ring current was observed for **NG1**.

The UV-Visible absorption spectra of **NG1** and **NG2** in toluene (Fig. 2a) exhibit strong, well-defined absorption bands at $\lambda < 400$ nm, closely resembling the high-energy features of the proligand **7** (Fig. S2). In contrast to **7**, **NG1** and **NG2** display additional lower-energy bands in the visible region (Table S2). **NG1** shows bands at λ = 498 (ε = 17 100) and 550 nm (6600 M^{-1} cm^{-1}), the latter tailing to around 600 nm, whereas those of **NG2** are hypsochromically shifted to λ = 476 (ε = 15 300) and 499 nm (15 800 M^{-1} cm^{-1}).

TDDFT calculations revealed that, for both the complexes and the ligand, the higher-energy absorption arises predominantly from nanographene-centered ππ* transitions. The additional low-energy bands observed for **NG1** and **NG2** originate from the two lowest-energy excitations (no. 1 and 2, Fig. 2) of mixed ππ* and intraligand charge-transfer (ILCT) character, resulting from conjugation between the isoquinoline and nanographene fragments and helicenic moiety formed upon cyclization combined with the introduction of the platinum (**NG1**) or boron (**NG2**). In **NG1**, these excitations also include metal-to-ligand CT (MLCT) contributions, resulting in the appearance of the low-energy band at 550 nm, for which there is no apparent counterpart in **NG2** or **7**. More details of the assignments and computational methodology can be found in the SI Section S4.

The ECD of **NG1** and **NG2** were measured in the same conditions (Fig. 2c and 2b respectively). In each case, the enantiopure (*P*) and (*M*) forms display mirror-image spectra, which were assigned by TDDFT calculations (see SI Section S4). **NG1** exhibits its strongest Cotton effect at 388 nm and its lowest energy band at 560 nm, whereas the corresponding features for **NG2** occur at 373 nm and 515 nm, respectively, with the lowest-energy ECD intensity governed by the aforementioned excitations no. 1 and 2 (see SI Section S4). Consistent with the absorption data (*vide supra*), the ECD spectrum of **NG1** is significantly bathochromically shifted relative to that of **NG2**. Similar absorption dissymmetry factors were obtained for both NGs, with g_{abs} = 0.0015 (435 nm) and g_{abs} = 0.0010 (408 nm) for **NG1** and **NG2**, respectively (Fig. S8 and S12).

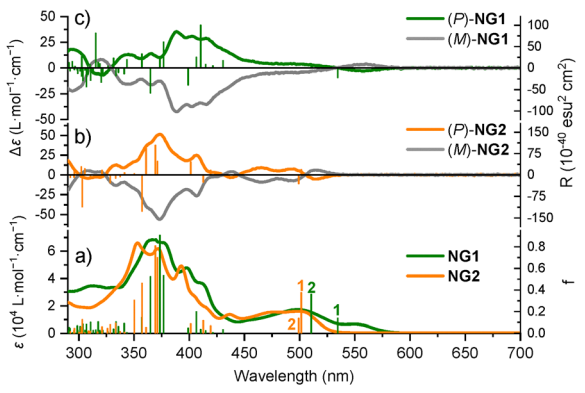

Fig. 2 (a) UV-Vis absorption of **NG1** and **NG2** along with (b) ECD spectra of enantiopure (*P*)- and (*M*)-**NG2** and (c) of (*P*)- and (*M*)-**NG1** (c), recorded in toluene, C ≈ 10^{-5} M. Bars indicate TDDFT-calculated excitation energies along with oscillator (a) and rotatory strengths (b) and (c).

Both nanographenes are luminescent in toluene at room temperature (Fig. 3a and Table S2). **NG1** emits at very low energy: almost all of its integrated emission lies at $\lambda > 700$ nm, in the NIR region, with only the onset falling into the deep red, showing the advantage of integrating a platinum center to red-shift the emission of the nanographene. There is a hint of vibrational structure, which becomes better resolved in the slightly blue-shifted spectrum recorded at 77 K. The emission lifetimes of 700 and 1200 ns recorded at 295 and 77 K respectively are consistent with phosphorescence from a triplet state, as is the significant quenching by oxygen observed in air-equilibrated solution (Fig. 3a). The emission is, however, weak, with a quantum yield Φ_{lum} in deoxygenated solution at 295 K of 0.33%. Efficient non-radiative decay through vibrational quenching is typical for low-energy emitters, suppressing quantum yields. Nevertheless, the fact that the lifetime is only modestly increased at 77 K suggests that a particularly low radiative rate constant k_r may also be a limiting factor. Indeed, if it assumed that the emissive state is formed with unit efficiency such that $k_r = \Phi_{lum}/\tau$, we can estimate k_r to be about 4700 s^{-1}, which is much lower than the values $\geq 10^5$ s^{-1} that are found for efficient green-emitting Pt(II) and Ir(III)-based phosphors. Low k_r values for phosphorescent organometallics are typically indicative of relatively inefficient SOC pathways, and often arise in complexes with extended conjugation, due to poor energy matching of the highest filled ligand orbitals with those of the metal.[37,38]

In contrast, **NG2** displays bright green emission in solution, with λ_{max} of 529 nm in deoxygenated toluene at 295 K, and a high quantum yield of 53% that is only marginally reduced upon aeration. The emission lifetime of 9.3 ns is indicative of fluorescence, and the estimated k_r of around 6 × 10^7 s^{-1} supports a spin-allowed origin for the emission, in contrast to the phosphorescent Pt(II) analogue. As observed for the phosphorescence of **NG1**, the fluorescence of **NG2** is a little blue-shifted at 77 K (as is normal for aromatics in the more rigid environment of a frozen glass), and vibrational structure becomes well resolved. The vibrational progression of around 1100 cm^{-1} is similar for **NG1** and **NG2**, and evidently associated with the C=C bonds of the highly conjugated helicene and nanographene systems. Finally, TDDFT calculations reasonably reproduce the measured fluorescence and phosphorescence energies of **NG1** (and its precursor **8**), **NG2**, and their parent ligand **7**, linking the experimental trends to increased ILCT character (and MLCT for **NG1** and **8**) of the corresponding excited states in the complexes (see SI Section S4).

The circularly polarized emission of the novel NGs was subsequently examined (Fig. 3b and c). Both enantiomers of

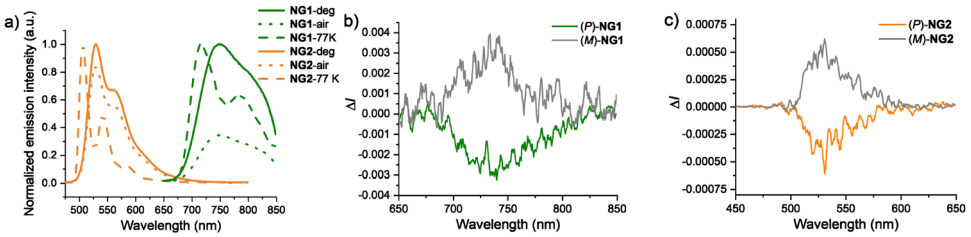

Fig. 3 (a) Emission spectra of **NG1** (orange) and **NG2** (green) in deoxygenated and air-equilibrated toluene at 295 K (plain and dotted lines respectively, plotted on the same intensity scale, λ_{ex} = 405 nm) and in a diethyl ether/isopentane/ethanol (2 : 2 : 1 v/v) mixture at 77 K (dashed lines). (b) CPL spectra of enantiopure (*P*)- and (*M*)-**NG1** (deoxygenated toluene, λ_{ex} = 500 nm, 20 °C, C ≈ 10^{-5} M). (c) CPL spectra of enantiopure (*P*)- and (*M*)-**NG2** (toluene, λ_{ex} = 353 nm, 20 °C, C ≈ 10^{-5} M).

Open Access Article. Published on 30 March 2026. Downloaded on 5/31/2026 11:00:37 AM.
This article is licensed under a Creative Commons Attribution 3.0 Unported Licence.

each NG derivative were studied in *ca.* 10^{-5} M toluene solutions (degassed for **NG1**, under air for **NG2**) and, as expected, each pair displayed mirror-image spectra. The CPL signals for **NG1** (Fig. 3b) span the range 690–810 nm, with a maximum at 740 nm and g_{lum} = 4 × 10^{-3} (Fig. S10), which is in the g_{lum} range of many efficient chiral phosphors (Table S1). The CPL of **NG2** (Fig. 3c) ranges from 500 to 600 nm, peaking at 530 nm, with a g_{lum} = 6 × 10^{-4} (Fig. S14). This order-of-magnitude difference in g_{lum} may arise from the distinctly different natures of the emitting states. **NG1** emits from a formally spin-forbidden T_1 state localized mainly on the newly formed helicenic system and of predominantly $^3\pi\pi^*/^3$MLCT character (with some ^{3}ILCT), whereas **NG2** emits from lowest-energy singlet state(s) dominated by (quinoline → NG) ^{1}ILCT. Note that the magnitude (and sign) of CPL might also be shaped by vibronic effects.[39,40] No CPL signal could be recorded for the NG-Pt(dmso)(Cl) **8**, possibly due to its emission being very weak (Table S2).

In conclusion, the first metal-containing chiral nanographene, **NG1**, has been synthesized and characterized, thereby providing a new class of helically chiral, heavy-atom-containing polyaromatic systems. The platinum(II) center (compared to boron) establishes more effective π-conjugation within the newly formed helix and promotes efficient intersystem crossing to populate triplet states manifold, which results in NIR phosphorescence (λ_{max} = 749 nm, emitting to >850 nm). Most significantly, **NG1** also functions as an efficient chiral phosphor. It exhibits a high g_{lum} of 4 × 10^{-3}, nearly an order of magnitude greater than that of its boron-containing fluorescent analogue **NG2** (g_{lum} = 6 × 10^{-4}). This pronounced chiroptical activity might be connected to localization of the emissive $^3\pi\pi^*/^3$MLCT state at the helical scaffold. This work validates a powerful molecular design strategy, with direct integration of heavy atoms into a chiral nanographene framework, and it demonstrates the potential for accessing high-performance CPL materials operating in the biologically relevant NIR window.

Conflicts of interest

The authors declare no conflict of interest.

Data availability

The data that support the findings of this study are available in the supplementary information (SI) section. Supplementary information: experimental procedures, photophysical and X-ray data, NMR spectra, HPLC analysis, computational details and calculated data. See DOI: https://doi.org/10.1039/d6cc00576d.

CCDC 2502439 (**NG1**) contains the supplementary crystallographic data for this paper.[41]

Acknowledgements

This work was supported by the Ministère de la Recherche et de l'Enseignement Supérieur, the Centre National de la recherche Scientifique (CNRS), the China-French associated international program in 'Functional Organophosphorus Materials', the Chinese Scholarship Council (CSC) and the French National Agency (ANR projects LumoMat-E, 18-EURE-0012). Y. G. acknowledges financial support from the Région Bretagne (SAD 2023_CNRS_PITCH). Elsa Caytan is thanked for her assistance with NMR measurements. Part of this work has been performed using the RennesMR core facility (ScanMAT, UAR 2025 Univ Rennes-CNRS, France). M. S.-H. gratefully acknowledges the Polish high-performance computing infrastructure PLGrid (HPC Centers: ACK Cyfronet AGH, CI TASK) for providing computer facilities and support within computational grants no. PLG/2024/017254 and PLG/2025/018408. A part of the computational study was carried out using research infrastructure funded by the European Union in the framework of the Smart Growth Operational Programme, Measure 4.2; Grant No. POIR.04.02.00-00-D001/20, "ATOMIN 2.0 – Center for materials research on ATOMic scale for the INnovative economy".

References

1 P. Izquierdo-García, J. M. Fernández-García, I. Fernández, J. Perles and N. Martín, *J. Am. Chem. Soc.*, 2021, **143**, 11864–11870.
2 Y. Gu, Z. Qiu and K. Müllen, *J. Am. Chem. Soc.*, 2022, **144**, 11499–11524.
3 S. Míguez-Lago, J. P. Mora-Fuentes, C. M. Cruz and A. G. Campaña, *Helicenes*, John Wiley & Sons, Ltd, 2022, pp. 283–328.
4 V. Kumar, J. L. Páez, S. Míguez-Lago, J. M. Cuerva, C. M. Cruz and A. G. Campaña, *Chem. Soc. Rev.*, 2025, **54**, 4922–4947.
5 W. Yang, Z. Ren, J. Feng, Z. Lv, X. Cheng, J. Zhang, D. Du, C. Chi and J. Shen, *Angew. Chem., Int. Ed.*, 2024, **63**, e202412681.

 This journal is © The Royal Society of Chemistry 2026

Open Access Article. Published on 30 March 2026. Downloaded on 5/31/2026 11:00:37 AM.
This article is licensed under a Creative Commons Attribution 3.0 Unported Licence.

6 P. J. Evans, J. Ouyang, L. Favereau, J. Crassous, I. Fernández, J. Perles and N. Martín, *Angew. Chem., Int. Ed.*, 2018, **57**, 6774–6779.
7 V. Kumar, G. Venugopal, A. B. Jadhav, S. D. Dongre, R. Gonnade, J. Kumar, P. C. Ruer, B. Hupp, A. Steffen and S. S. Babu, *Angew. Chem., Int. Ed.*, 2025, **64**, e202422125.
8 G. Venugopal, V. Kumar, A. Badrinarayan Jadhav, S. D. Dongre, A. Khan, R. Gonnade, J. Kumar and S. Santhosh Babu, *Chem. – Eur. J.*, 2024, **30**, e202304169.
9 F. Gan, C. Shen, W. Cui and H. Qiu, *J. Am. Chem. Soc.*, 2023, **145**, 5952–5959.
10 P. Izquierdo-García, J. M. Fernández-García, S. Medina Rivero, M. Šámal, J. Rybáček, L. Bednárová, S. Ramírez-Barroso, F. J. Ramírez, R. Rodríguez, J. Perles, D. García-Fresnadillo, J. Crassous, J. Casado, I. G. Stará and N. Martín, *J. Am. Chem. Soc.*, 2023, **145**, 11599–11610.
11 *Molecular nanographenes: Synthesis, properties, and applications*, ed. N. Martin and C. P. Nuckolls, Blackwell Verlag, Berlin, Germany, 2025.
12 P. Izquierdo-García, J. Lión-Villar, J. M. Fernández-García and N. Martín, *Chem. Soc. Rev.*, 2025, **54**, 11089–11104.
13 G.-F. Huo, W.-T. Xu, J. Hu, Y. Han, W. Fan, W. Wang, Z. Sun, H.-B. Yang and J. Wu, *Angew. Chem., Int. Ed.*, 2025, **64**, e202416707.
14 Y. Hu, G. M. Paternò, X.-Y. Wang, X.-C. Wang, M. Guizzardi, Q. Chen, D. Schollmeyer, X.-Y. Cao, G. Cerullo, F. Scotognella, K. Müllen and A. Narita, *J. Am. Chem. Soc.*, 2019, **141**, 12797–12803.
15 J. Tan, X. Xu, J. Liu, S. Vasylevskyi, Z. Lin, R. Kabe, Y. Zou, K. Müllen, A. Narita and Y. Hu, *Angew. Chem., Int. Ed.*, 2023, **62**, e202218494.
16 Y.-Y. Ju, J.-F. Xing, Y.-M. Xie, X.-F. Li, X.-J. Zhao, G.-H. Nie, B. Zhang and Y.-Z. Tan, *J. Am. Chem. Soc.*, 2025, **147**, 45514–45522.
17 H. He, J. Lee, Z. Zong, N. Liu, Y. Noh, V. M. Lynch, J. Oh, J. Kim, J. L. Sessler and X.-S. Ke, *Nat. Commun.*, 2025, **16**, 1534.
18 R. N. Schaugaard, K. Raghavachari and L. Li, *Inorg. Chem.*, 2018, **57**, 10548–10556.
19 H. Yersin, *Highly efficient OLEDs with phosphorescent materials*, Wiley-VCH, Weinheim, 2008, ch 1 and 7.
20 Y. Zhang, W. Fu, X. Feng, Y. Ma, W. Yu, N. Yang and C. Shen, *J. Mol. Struct.*, 2026, **1356**, 145112.
21 X. Qiao, Q. Li, R. N. Schaugaard, B. W. Noffke, Y. Liu, D. Li, L. Liu, K. Raghavachari and L. Li, *J. Am. Chem. Soc.*, 2017, **139**, 3934–3937.
22 P. Vázquez-Domínguez, M. Horojat, E. Suits, F. J. F. de Córdova, N. Vanthuyne, D. Jacquemin, A. Ros and L. Favereau, *Mater. Chem. Front.*, 2024, **8**, 3799–3806.
23 L. Norel, M. Rudolph, N. Vanthuyne, J. A. G. Williams, C. Lescop, C. Roussel, J. Autschbach, J. Crassous and R. Réau, *Angew. Chem., Int. Ed.*, 2010, **49**, 99–102.
24 E. Anger, M. Rudolph, C. Shen, N. Vanthuyne, L. Toupet, C. Roussel, J. Autschbach, J. Crassous and R. Réau, *J. Am. Chem. Soc.*, 2011, **133**, 3800–3803.
25 C. Shen, E. Anger, M. Srebro, N. Vanthuyne, K. K. Deol, T. D. Jefferson, G. Muller, J. A. G. Williams, L. Toupet, C. Roussel, J. Autschbach, R. Réau and J. Crassous, *Chem. Sci.*, 2014, **5**, 1915–1927.
26 J. R. Brandt, X. Wang, Y. Yang, A. J. Campbell and M. J. Fuchter, *J. Am. Chem. Soc.*, 2016, **138**, 9743–9746.
27 Z.-P. Yan, X.-F. Luo, W.-Q. Liu, Z.-G. Wu, X. Liang, K. Liao, Y. Wang, Y.-X. Zheng, L. Zhou, J.-L. Zuo, Y. Pan and H. Zhang, *Chem. – Eur. J.*, 2019, **25**, 5672–5676.
28 A. Nowak-Król, P. T. Geppert and K. R. Naveen, *Chem. Sci.*, 2024, **15**, 7408–7440.
29 M. Schnitzlein, K. Shoyama and F. Würthner, *Chem. Sci.*, 2024, **15**, 2984–2989.
30 C. Shen, M. Srebro-Hooper, M. Jean, N. Vanthuyne, L. Toupet, J. A. G. Williams, A. R. Torres, A. J. Riives, G. Muller, J. Autschbach and J. Crassous, *Chem. – Eur. J.*, 2017, **23**, 407–418.
31 F. Full, Q. Wölflick, K. Radacki, H. Braunschweig and A. Nowak-Król, *Chem. – Eur. J.*, 2022, **28**, e202202280.
32 F. Full, A. Artigas, K. Wiegand, D. Volland, K. Szkodzińska, Y. Coquerel and A. Nowak-Król, *J. Am. Chem. Soc.*, 2024, **146**, 29245–29254.
33 A. F. Palermo, B. S. Y. Chiu, P. Patel and S. A. L. Rousseaux, *J. Am. Chem. Soc.*, 2023, **145**, 24981–24989.
34 R. Nagpal, S. Arora, P. Ponnan, K. Nisa, A. Dandia and S. M. Singh Chauhan, *ChemistrySelect*, 2019, **4**, 8444–8449.
35 R. H. Martin, *Angew. Chem., Int. Ed. Engl.*, 1974, **13**, 649–660.
36 A. R. Krappe, J. C. Mayer, W. Zhang, L. M. Filla, G. Ligorio, F. Hermerschmidt, L. S. Eitelhuber, A. Güttler, M. Weber, B. Paulus, U. Resch-Genger, E. J. W. List-Kratochvil and S. Eigler, *Chem. – Eur. J.*, 2025, **31**, e202500742.
37 D. N. Kozhevnikov, V. N. Kozhevnikov, M. Z. Shafikov, A. M. Prokhorov, D. W. Bruce and J. A. Gareth Williams, *Inorg. Chem.*, 2011, **50**, 3804–3815.
38 P. Pander, R. Daniels, A. V. Zaytsev, A. Horn, A. Sil, T. J. Penfold, J. A. G. Williams, V. N. Kozhevnikov and F. B. Dias, *Chem. Sci.*, 2021, **12**, 6172–6180.
39 Y. Liu, J. Cerezo, G. Mazzeo, N. Lin, X. Zhao, G. Longhi, S. Abbate and F. Santoro, *J. Chem. Theory Comput.*, 2016, **12**, 2799–2819.
40 T. Mori, *Angew. Chem., Int. Ed.*, 2024, **63**, e202319702.
41 CCDC 2502439: Experimental Crystal Structure Determination, 2026, DOI: 10.5517/ccdc.csd.cc2pzzvj.